NeuroImage 172 (2018) 632–641

Contents lists available at ScienceDirect

NeuroImage

journal homepage: www.elsevier.com/locate/neuroimage

"Brain over body"–A study on the willful regulation of autonomic function during cold exposure

Otto Muzik [a,b,*], Kaice T. Reilly [c], Vaibhav A. Diwadkar [d]

[a] Departments of Pediatrics, Wayne State University School of Medicine, Detroit, MI 48201, USA
[b] Departments of Radiology, Wayne State University School of Medicine, Detroit, MI 48201, USA
[c] TKR Research and Consulting, LLC, Detroit 48201 USA
[d] Departments of Psychiatry and Behavioral Neurosciences, Wayne State University School of Medicine, Detroit, MI 48201, USA

ARTICLE INFO

Keywords:
Wim Hof method
CNS thermoregulation
Cold exposure
Functional MRI
FDG PET
Hydroxyephedrine PET
Stress-induced analgesia
Periaqueductal gray

ABSTRACT

The defense of body temperature against environmental thermal challenges is a core objective of homeostatic regulation governed by the autonomic nervous system. Autonomous mechanisms of thermoregulation are only weakly affected by top-down modulation, allowing only transient tolerance for extreme cold. There is however, anecdotal evidence of a unique set of individuals known for extreme cold tolerance. Here we present a case study of a 57-year old Dutch national, Wim Hof, the so-called "Iceman", with the ability to withstand frequent prolonged periods of extreme cold exposure based on the practice of a self-developed technique involving a combination of forced breathing, cold exposure and meditation (collectively referred to as the Wim Hof Method, henceforth "WHM"). The relative contributions of the brain and the periphery that endow the Iceman with these capabilities is unknown. To investigate this, we conducted multi-modal imaging assessments of the brain and the periphery using a combination of fMRI and PET/CT imaging. Thermoregulatory defense was evoked by subjecting the Iceman (and a cohort of typical controls) to a fMRI paradigm designed to generate periods of mild hypothermia interspersed by periods of return to basal core body temperature. fMRI was acquired in two separate sessions: in a typical (passive) state and following the practice of WHM. In addition, the Iceman also underwent a whole body PET/CT imaging session using the tracers C11-hydroxyephedrine (HED) and 18F-fluorodeoxyglucose (FDG) during both thermoneutral and prolonged mild cold conditions. This acquisition allowed us to determine changes in sympathetic innervation (HED) and glucose consumption (FDG) in muscle and fat tissues in the absence of the WHM. fMRI analyses indicated that the WHM activates primary control centers for descending pain/cold stimuli modulation in the periaqueductal gray (PAG), possibly initiating a stress-induced analgesic response. In addition, the WHM also engages higher-order cortical areas (left anterior and right middle insula) that are uniquely associated with self-reflection, and which facilitate both internal focus and sustained attention in the presence of averse (e.g. cold) external stimuli. However, the activation of brown adipose tissue (BAT) was unremarkable. Finally, forceful respiration results in increased sympathetic innervation and glucose consumption in intercostal muscle, generating heat that dissipates to lung tissue and warms circulating blood in the pulmonary capillaries. Our results provide compelling evidence for the primacy of the brain (CNS) rather than the body (peripheral mechanisms) in mediating the Iceman's responses to cold exposure. They also suggest the compelling possibility that the WHM might allow practitioners to develop higher level of control over key components of the autonomous system, with implications for lifestyle interventions that might ameliorate multiple clinical syndromes.

Introduction

Defending body temperature against environmental thermal challenges is one of the most fundamental of homeostatic functions governed by the central nervous system (CNS) and has high adaptive significance. In addition to triggering thermoregulatory responses, cold exposure generates aversive feelings that mediate behavioral avoidance. This cascade of events induces avoidance that pre-empts the potentially tissue-damaging effects of cold exposure challenge. Thus, stress-induced suppression of sensitivity to external aversive stimuli is an in-built

* Corresponding author. PET Center, Children's Hospital of Michigan, 3901 Beaubien Blvd, Detroit, MI 48201, USA.
E-mail address: otto@pet.wayne.edu (O. Muzik).

https://doi.org/10.1016/j.neuroimage.2018.01.067
Received 16 June 2017; Accepted 26 January 2018
Available online 10 February 2018
1053-8119/

mammalian mechanism that might be thought of as a component of the fight and flight response. Human biological adaptability, genetics and natural selection can all modify or mediate some of these responses (Hancock et al., 2008; Lasker, 1969; Racimo et al., 2017) but within a limited range. In general, extreme abilities to withstand cold exposure rarely emerge within the lifespan of individuals as thermoregulatory mechanisms are largely autonomous and not subject to willful and/or tonic modification (Daanen and Van Marken Lichtenbelt, 2016). Nevertheless, evidence exists of individuals with extreme and inexplicable cold tolerance significantly outside of typical limits, yet they have rarely been subjected to scientific inquiry, and never to neuroimaging.

With these issues in mind, here we present a case study of a 57-year old Dutch national, the so-called "Iceman", who can withstand frequent prolonged periods of extreme cold exposure. This tonic capability in the Iceman appears to result from the rigorous self-application of a specially developed technique (the Wim Hof Method, WHM). The WHM consists of the daily practice of a combination of three main elements: a) initial forced breathing (several rounds of hyperventilation followed by breath retention and deep inhalations and exhalations), b) followed by exposure to cold (e.g. whole body exposure to ice-cold water or walking in cold environment bare-chested) and c) mindful body awareness focus on deep breathing (Kox et al., 2014). The Iceman is the world-record holder in several cold challenges, such as the fastest half-marathon on snow and ice while barefoot, and the longest duration while fully immersed in crushed ice (1 h and 50 min). Practice of the WHM appears to allow him to regulate his autonomic NS in the presence of severe cold. For example, a recent case study demonstrated that he could control his autonomic stress response during endotoxemia (Kox et al., 2014), indicating the ability of this method to modulate the innate immune response. Pertinent to our investigation, practice of the WHM has endowed the Iceman with remarkable tonic propensity for thermoregulatory defense. This endowment, and his putative brain and body responses to cold exposure must be reconciled and compared with recent in vivo studies in typical volunteers.

Recent studies have begun to detail functional MRI (fMRI) estimated response in CNS pathways to experimentally induced changes in body temperature (Muzik and Diwadkar, 2016). These studies have shown that controlled whole body cold exposure drives responses of homeostatic nuclei within the brainstem that mediate autonomic CNS responses to peripheral inputs (Satinoff, 1978). Additional naturalistic studies of endogenous thermoregulatory events have identified contributions from higher-order cortical areas such as the insular cortex, the anterior cingulate, the posterior parietal somatosensory cortex, and especially the orbitofrontal cortex. These regions collectively constitute networks for the interoception of the body's internal states and a value-generating network that guides behavior (Craig, 2002; Diwadkar et al., 2014). These "higher order" regions have a marginal (if any) modulatory effect on the autonomic NS, with no known direct anatomical pathways that can sub-serve interaction. However, anecdotal evidence suggests that top-down regulation might assume a much larger role in the autonomic regulatory cascade as previously assumed, even though these mechanisms remain subject to more systematic discovery.

His unique abilities make the Iceman an important specimen that allows investigation of highly adapted human thermoregulatory mechanisms, having provided important insights into physiology (Kox et al., 2012, 2014). Yet, imaging-driven insights into processes in the CNS and the periphery are either absent (brain) or limited (body) (Vosselman et al., 2014). In light of the above considerations, our study was designed to study the relationship between conscious and autonomic aspects of CNS function (represented in cortical and sub-cortical regions), and their comparative effects relative to the periphery during an oscillating cold thermal challenge. Imaging data obtained for the Iceman was compared to data acquired under identical challenges in a group of controls. By exploring CNS responses to cold exposure in this unique individual relative to a normative population, our objective was to discover the underlying correlates of cold resilience in the brain and body. The strength of this approach is that it relates the interpretation of the fMRI data (acquired in the CNS) to a specific physiological context (acquired in the periphery using PET imaging). Our results indicate that while his body's responses to our applied thermal stressor (in terms of activated brown adipose tissue) was relatively unremarkable, his brain showed substantially different functional responses during thermoregulatory challenge.

Material and methods

Subjects

The Human Investigation Committee of Wayne State University authorized the study and informed written consent was obtained from all participants. Study participants were screened for medical history and metabolic status, as assessed on the basis of routine laboratory tests and measured blood pressure. The Iceman and controls underwent a well-established research protocol established in our Imaging Center (Muzik et al., 2017) (see Table 1). For all participants body mass index (BMI) was calculated as weight/height2 (kg/m^2), and percent body fat (%) was calculated from the sum of skinfold measurements at the biceps, triceps, subscapular and suprailiac sites using Lange calipers. The lean body mass (LBM; kg) was subsequently calculated as body weight less fat mass. Although the control group was significantly younger than the Iceman, the rate-pressure product (representing myocardial workload which is directly related to hemodynamic response) was similar.

Study design

To assess functional brain responses to cold stress, the "Iceman" underwent a fMRI paradigm on two separate days. On each day, the fMRI paradigm consisted of an oscillating whole body temperature challenge designed to generate periods of mild hypothermia interspersed by periods of return to basal core body temperature (see below). The Day 1 acquisition was in a pre-scan "passive" state. The Day 2 acquisition followed the pre-scan practice of the WHM. The neuroimaging studies were complemented by scans of the periphery. Thus, on a third day the Iceman underwent a whole-body PET/CT imaging session using the tracers C11-hydroxyephedrine (HED) and 18F-fluorodeoxyglucose (FDG) during both thermoneutral (rest) and mild cold conditions also in a "passive" state. He was specifically instructed to not use the WHM prior or during the entire PET/CT protocol to allow assessment of peripheral tissue response to sympathetic activation during a baseline "passive" condition. This PET/CT protocol has been used in our Imaging Center in the past to study the effects of sympathetic stimulation on cold-induced activation of brown adipose tissue (BAT) (Muzik et al., 2012, 2013). During the protocol, whole body changes in daily energy expenditure (DEE, kcal/day) between the cold and thermoneutral conditions were assessed using indirect calorimetry and related to changes in PET tracer accumulation (HED and FDG). By definition, our typical controls having not been trained in the WHM, thus all fMRI and PET data in the control group was obtained in a "passive" state.

Mild cold exposure during both PET and fMRI acquisitions was

Table 1
Descriptive Statistics for the Iceman and the Control group.

Parameter	Iceman	Controls	range [min – max]
Subjects		20 (10 F/10 M)	
Age (years)	57	23.3 ± 3.8	19–32[a]
Height (cm)	182	172 ± 12	152–198
Weight (kg)	86	69 ± 16	53–101
BMI (kg/m^2)	25.9	23.0 ± 2.6	19.6–26.9
Body Fat (%)	28	25.4 ± 5.8	16–32
LBM (kg)	61.9	54.5 ± 14.5	38.8–84.7
RPP (min mmHg)	7191	7572 ± 1273	9325 - 4826

[a] Significant at the 0.05 level; RPP: rate-pressure product.

applied using a specially designed whole-body garment (Muzik and Diwadkar, 2016). In brief, the garment includes a network of small-diameter plastic tubing woven into the fabric (Allen Vanguard, Inc. Ottawa, CA) through which temperature-controlled neutral (31–34 °C) or cold water (15–17 °C) is circulated from two separate water reservoirs. Skin temperature is monitored using a GaAs crystal sensor located at the tip of an optical fiber cable (OpSense, Inc. Quebec City, CA), allowing accurate measurement of temperature (to within 0.1 °C) inside the MR scanner. The sensor was taped to the skin at the location of the left rib cage. This location was selected based on its proximity to important anatomical features (close to the pulmonary blood vessels which are highly representative of core body temperature) and the ability to consistently place the sensors based on the anatomical landmark (Xu et al., 2013). Both the Iceman and control subjects were closely monitored during the cold exposure period for signs of shivering. In addition to physiological monitoring of skin temperature, every 5 min subjects reported about his/her subjective feeling of cold. In the case that shivering was on the cusp of occurring based on the subject's self-report, the water temperature in the garment was raised to pre-empt this.

MRI procedure

Structural and functional MRI data acquisition was performed on a 3T Siemens Verio system using a 12-channel volume head coil. Initially, a 3D T1-weighted anatomical MRI sequence was acquired (TR: 2200 ms, TI: 778 ms, TE: 3 ms, flip-angle = 13°, FOV: 256 × 256mm^2, 256 axial slices of thickness = 1.0 mm, matrix = 256 × 256, scan-time = 5min 22 s). Subsequently, a gradient echo EPI fMRI data acquisition was conducted (TR: 2.6s, TE: 29 ms, FOV: 256 × 256mm^2, acquisition matrix: 128 × 128, 36 axial slices, voxel dimensions: 2 × 2 x 3mm^3). These parameters allow acquisition of fMRI data with high in vivo spatial resolution. The total study time was ~1 h.

The fMRI paradigm consisted of 600 images (TR = 2.6s) resulting in a 25-min sequence blocked into five 5-min epochs. The epochs alternated between the neutral and cold stimulus. The paradigm is schematically depicted in Fig. 1.

PET data acquisition

All subjects were scanned using a GE Discovery STE PET/CT scanner in 3D mode following a >6 h fasting period. A venous catheter was established for tracer injection and arterial oxygen saturation (pSat) was monitored during the whole protocol using a Dinamap ProCare 400 monitor (GE Healthcare). The protocol started with two low-level CT scans (100 kVp, 60 mA) for attenuation correction, one at the location of the supraclavicular BAT region (also including the ascending aorta inferior to the aortic arch) and the other at the level of subcutaneous white adipose tissue (WAT) in the lower abdomen (including the descending aorta). After acquisition of the CT transmission scans, the norepinephrine analog 11C-*meta*-hydroxyephedrine (HED) was injected (370 MBq) as a slow bolus over 20 s. Coinciding with the tracer injection, a dynamic scan was initiated (12 × 10, 3 × 60, and 4 × 300 s). Following conclusion of the dynamic scan, the patient was repositioned with the lower abdomen in the FOV, and a static scan (8 min) of abdominal WAT was obtained. During the entire baseline protocol, subjects were kept in a thermoneutral condition by maintaining the suit water temperature at 31°C–34 °C.

Following the baseline protocol, subjects were exposed to mild cold temperature for the rest of the study (~3 h) by changing the circulating water temperature to 15°C–17 °C. After a cooling period of at least 1 h duration, the baseline protocol was repeated. At its conclusion, the 18F-FDG tracer (150 MBq) was injected, and after a 45-min uptake period a 5 bed-position PET/CT scan was acquired, covering the torso from the neck to the lower abdomen. All PET emission data was corrected for attenuation, scatter, and random events and then iteratively reconstructed into 128 × 128 x 47 matrices (voxel dimensions, 5.47 × 5.47 × 3.27 mm) using the ordered-subset expectation maximization (OSEM) algorithm (2 iterations, 20 subsets and post-processing gaussian filter with 6.0 mm in full width at half maximum). The final spatial resolution of the image volumes was ~7 mm full width at half maximum (FWHM).

PET data analysis

Previous mechanistic studies of the HED tracer have established high neuronal selectivity, long neuronal retention times, and a correlation between tissue retention of tracer and tissue norepinephrine concentration (Rosenspire et al., 1990). To calculate the HED retention index (RI), the arterial input functions need to be known. The validity of an image-derived input function obtained from the ascending aorta (AA) for accurate quantification of myocardial perfusion has been shown in several 15O-water studies that compared flow values obtained using the image-derived input function with those determined using arterial blood sampling (Lubberink et al., 2010; van der Veldt et al., 2010). A 3D region of interest (ROI, 1 cm diameter) was defined over the AA using the AMIDE software, and spillover from the left atrium was avoided by considering only planes in which the left atrium was not visible. The resulting time–activity curve was subsequently corrected for partial-volume effects by accounting for the diameter of the AA obtained from CT (2.3 + 0.3 cm) and the FWHM of the reconstructed PET images (Germano et al., 1992). To extrapolate the AA time-activity curve beyond

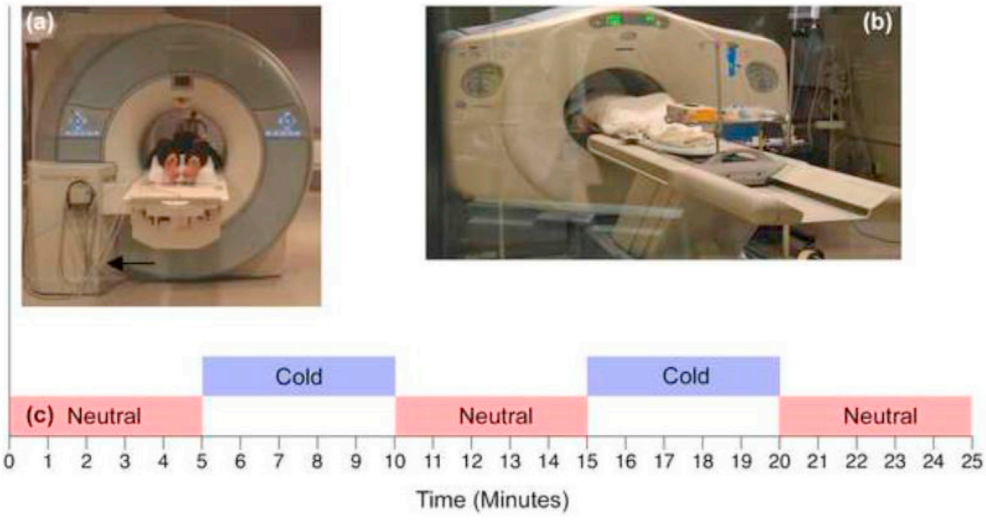

Fig. 1. The figure schematically depicts the experimental setup and overview of the experimentally control administration of the cold stress paradigm (for fMRI). (a) In this picture of an acquisition, the Iceman is shown prone in the bore of the MR scanner clad in the specially designed whole body garment. The arrow points to the visible tubing through which temperature controlled water was infused into the garment from reservoirs in the control room. (b) This picture of the PET acquisition shows the Iceman prone in the bore of the PET/CT scanner. Note that the PET data was acquired following the administration of cold stress. (c) The temperature controlled water was infused to create a paradigm that oscillated between infusions of neutral temperature water (31–34 °C) or cold water (15–17 °C). The fMRI paradigm lasted 25 min.

the initial 25 min, the curve was fitted with a tri-exponential function, and the slowest exponential was used for continuation of the input function up to 40 min after injection. An analogous approach was used for the abdominal scans using the descending aorta (DA). It has been shown that this method is in good agreement with the arterial function, because the DA is relatively free of spillover from other organs and extends from the upper thorax to the lower abdomen (Ohtake et al., 1991). The ROIs representing supraclavicular BAT as well as subcutaneous WAT were defined in CT images based on the density of adipose tissue (−250 to −50 Hounsfield units). ROIs representing WAT were defined at the level of the lower abdomen superior to the hip joint. A ROI at the location of the deltoid muscle was assumed to be representative for superficial muscle tissue, whereas the psoas muscle was used to assess the activity of deep muscle tissue. Moreover, due to the central role of forced breathing in WHM, we also defined ROIs representing the superior (between the first and second rib) and inferior (between the fourth and fifth rib) intercostal muscle. ROIs were defined in CT transaxial images and included bilaterally the area between the ribs from the sternum to the spine, including both the external and internal muscle layers. Regional time-activity curves were derived from the dynamic HED scans and the HED RI was calculated as the quotient between the average HED tracer concentration in tissues at 30–40 min post-injection and the integral of HED tracer concentration in blood (Allman et al., 1993). Glucose metabolism in tissue was quantified from FDG images using the standard uptake value (SUV, defined as tracer concentration in MBq/cc normalized to injected activity (MBq) per weight (g)). Due to the limited axial coverage of a one-bed position dynamic scan, the HED RI was only calculated for the superior intercostal muscle.

Measurement of whole body indirect calorimetry

Measurement of energy expenditure (kcal/day) under resting (prior to cold exposure) and cold (90 min into cold exposure) conditions was performed using the MedGraphics VO2000 Portable Metabolic Testing System (St. Paul, MN). The instrument was calibrated against a known gas mixture prior to each experimental day, and auto-calibrated between experimental runs. For both conditions, subjects were measured while lying in a relaxed position, in a fasting state (≥6 h). Subjects were fitted with neoprene face masks, and all measurements were taken using the low flow pneumotachs. Heart rate (HR; beats/min), oxygen consumption (VO2; l/min), carbon dioxide production (VCO2; l/min) and respiratory quotient (RQ; VCO2/VO2) were all measured for 10 min. Whole body daily energy expenditure (DEE, kcal/d) was then calculated from VO2 and RQ values using the BreezeSuite software (Version 6.0; MedGraphics).

Statistical analysis

fMRI data

fMRI data was analyzed using SPM8 (Wellcome Department of Cognitive Neurology, Institute of Neurology, London, UK). In all analyses, the first four images were discarded to account for EPI equilibration effects. The remaining images in the sequence were realigned to correct for head movements, corrected for slice timing, and subsequently spatially normalized based on the transformation matrix derived between the coregistered (to the mean EPI sequence image) T1-weighted image volume and the MNI template brain. The images were then smoothed spatially with a 3D Gaussian kernel of 6 mm FWHM and resampled ($2 \times 2 \times 2\,mm^3$). A high-pass filter (cutoff 1/128 s) was employed to remove low-frequency signal drifts. Data was modeled voxel-wise, applying a general linear model (GLM) based on a boxcar waveform (derived from the previously described epochs modeled using skin temperature data) and convolved with the canonical hemodynamic response function. The confounding effect of global signal intensity was removed using proportional scaling. The first-level analysis included correction for within-scanner motion by means of 6 realignment parameters as regressors, which were derived from the initial realignment step.

Variations in fMRI responses under the different regimes from the skin temperature curve were modeled at the first level using pair-wise directional contrasts. Contrasts identified fMRI responses associated with cooling relative to warming. Thus, at the first level, the individual contrast images identified changes in the amplitude of activation profiles of brain regions during cooling relative to warming (Muzik and Diwadkar, 2016). These individual contrast images were subsequently analyzed using a second-level random-effects analysis (Turner et al., 1998), which separately assessed differences in activation between either the Iceman's "passive" or WHM condition against the control group's "passive" condition during the temporal windows of interest. Activations were assessed in the established and validated thermoregulatory-interoceptive network of regions including the brainstem, insula, anterior cingulate cortex, orbitofrontal cortex, posterior parietal cortex and the hypothalamus (Muzik and Diwadkar, 2016; Craig, 2002; Diwadkar et al., 2014). All analyses were constrained respecting the relative homogeneity of function within the regions of interest. Significant clusters within each region were identified using AlphaSim (Ward, 2000), by estimating the minimum cluster extent sufficient for activated clusters to be rejected as false positive (noise-only) clusters. This approach performs a Monte Carlo alpha probability simulation, by means of computing the probability of a random field of noise (after accounting for the spatial correlations of voxels based on the image smoothness within each region of interest estimated directly from the data set) to produce a cluster of a given size, after the noise is thresholded at a given level. Thus, instead of using the individual voxel probability threshold alone in achieving the desired overall significance level, the method uses a combination of both probability thresholding and minimum cluster size thresholding. The underlying principle adopts the stand that true regions of activation will tend to occur over contiguous voxels within a region of relative functional homogeneity, whereas noise has much less of a tendency to form clusters of activated voxels. Because recent reports have questioned the significance of activation foci based on cluster-defining thresholds (Eklund et al., 2016), all significant activation clusters were subsequently used as masks to extract the fMRI responses at each sampled time point across the whole study in each subject. Specifically, for each activation mask and subject, the first eigenvariate from the modeled fMRI time sequence was extracted and subsequently averaged over subjects, thus yielding a single time-series each for the Iceman and the control group respectively. These time series' represent the % signal change on a point-wise basis from the mean fMRI signal value. To report activation peaks, voxel coordinates in MNI space were transformed into Talairach space using a previously established algorithm (Lancaster et al., 2007) and Brodmann areas were reported where appropriate.

PET data

The Iceman's data was assessed against the typical control group as follows. Data from the control group was used to create boxplots that established the normal interquartile range as well as the extremes (minimum/maximum value). Such representation of the data is non-parametric, displaying variation in samples of a statistical population with no assumptions of the underlying statistical distribution. Values obtained for the Iceman that fell within the interquartile range of the control group were considered comparable to the controls. In contrast, values outside the extremes of the control group were deemed significantly different. Finally, values outside the interquartile range but still within the extremes of the control group were considered trend worthy.

Results

We organize the results as follows: We first present skin temperature data from the fMRI paradigm (Fig. 2) derived from typical controls and both of the Iceman's fMRI acquisitions ("passive" and WHM). We next show significant fMRI differences in activation in the brainstem and the

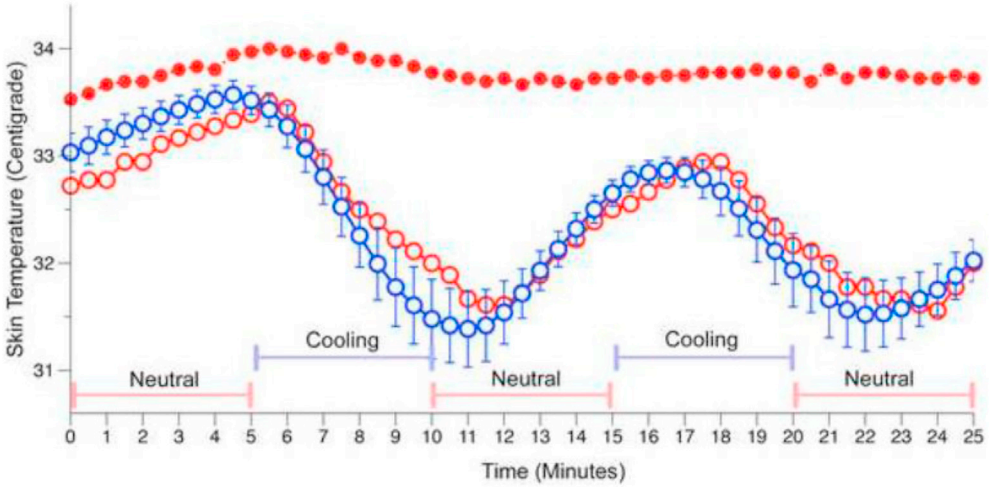

Fig. 2. Paradigm-induced changes in skin temperature. The three depicted curves show paradigm-induced changes in skin temperature in the typical controls (blue curve with open circles, error bars ± SD), the Iceman in the "passive" state (red curve with open circles), and the Iceman in the WHM state (red curve with closed circles). The bars above the x-axis (time), depict the time windows during which the suit was infused with neutral temperature water (31–34 °C) or cold water (15–17 °C). In the "passive" state, the Iceman's skin temperature curve was comparable to typical controls. The Iceman's skin temperature measured following WHM did not follow the oscillatory pattern observed during the "passive" condition, and he maintained basal skin temperature and could resist the cold stress challenge over 25 min (red curve closed circles).

insula regions between the Iceman and typical controls (Fig. 3; Table 2) during cooling. Finally, we present PET results (Figs. 4 and 5; Table 3) showing that responses within the Iceman's body were in general comparable to those found in typical controls.

Effects of the WHM on skin temperature

As shown in Fig. 2, the alternating stimulus induced skin temperature oscillations in an ~2 °C (~5 °F) range in both typical controls and the Iceman in the "passive" state, consistent with previously documented systematic (and phased delayed) oscillations in skin temperature. These curves for both typical controls and the Iceman in the "passive" state (Fig. 2, bottom) depict two broadly distinct skin-temperature regimes: A dynamic negative gradient associated with cooling and a dynamic positive gradient associated with warming (or return to neutral). These gradients reflect high rates of skin temperature change in response to the stimulus. Previous studies have indicated that the fMRI response is highly sensitive to the dynamics of skin temperature but not to relatively stable periods of cold or neutral skin temperatures (Muzik and Diwadkar, 2016). Thus, these distinct regimes constituted separable physiological predictors of the BOLD response, and were employed to construct epochs of interest for fMRI analyses for each of the Iceman's acquisitions. Each epoch was modeled with a temporal radius of 2 min centered at points of the highest rates of skin temperature change (in the negative or positive direction). For the Iceman's post-WHM acquisition, the temporal window from his "passive" acquisition was brought forward to the WHM acquisition. In each participant, these first level models estimated neuronal responses during (relatively) rapid skin temperature transitions when thermoregulatory demands were maximal.

Differences in brain responses during cooling

First-level analysis assessed contrasts associated with cooling relative to warming. Subsequently, a second-level random effects analysis compared contrast images derived from the control group against the contrast image obtained from the Iceman, separately for the "passive" and WHM acquisitions. The identified significant clusters in core autonomic brainstem and interoceptive limbic regions reflect differential responses to skin temperature changes during cooling and warming periods. The spatial profiles of the observed differences in activation are supplemented by the temporal profiles of the smoothed (using non-parametric local regression), LOESS (Cleveland and Devlin, 1988); activation time series. These curves permit an inspection of the differential ranges of the fMRI estimated neuronal response in the significant regions associated with cooling and warming. The reporting of results is organized by region.

Response profile in the brainstem

As seen in Fig. 3a, we determined a significant increase in BOLD signal at the location of the periaqueductal gray (PAG) area (Table 2) during cooling when comparing the Iceman's WHM condition against the control group's "passive" condition. To elucidate the basis of this effect, we depict the LOESS smoothed time series' across the entire experiment for both the Iceman ($R2 = 0.275$, $\sigma = 0.368$, s for residual = 0.3683) and the control group ($R2 = 0.2982$, $\sigma = 1.03$, s for residual = 1.03). The data reflects an approximately 3% increase during cold exposure, pointing towards a large-scale activation of the PAG region associated with the active (WHM) condition. No such activation in the PAG was observed in the control group. In contrast to the WHM condition, BOLD signal in the PAG region was slightly decreased when the Iceman was scanned during the "passive" condition, but no voxels survived the significance threshold. In addition, we observed a significant increase in BOLD signal in the pons, consistent with the location of mid-level deep pontine nuclei that are involved with physiological responses to stress, such as the parabrachial nucleus and the locus coeruleus.

Response profiles in the insula

The pattern of BOLD responses in the insula were complementary to those in the brainstem (Table 2). Activations at the location of the left anterior insula and the right middle insula (Fig. 3b) were found to be in opposite phase to those determined in the PAG. As seen from the accompanying graphs, the estimated neuronal response range between periods of skin cooling and warming was ~50% lower in the control group during rest as compared to that determined for the Iceman during the WHM condition. The LOESS smoothed fMRI response curves for the Iceman ($R2 = 0.313$, $\sigma = 0.964$, s for residual = 0.965) and the control group ($R2 = 0.398$, $\sigma = 0.485$, s for residual = 0.486) provide a temporal depiction of these effects. These effects are discussed in greater detail in the Discussion section. Finally, no significant differences were determined between the Iceman's "passive" condition and the control group data.

FDG PET results

Whole body FDG images of the Iceman obtained during mild cold exposure showed only a small amount of FDG uptake at the location of supraclavicular BAT (Fig. 4A). The total amount of cold-activated BAT was determined as 25 g, which lies slightly below the interquartile range

Figure 3

(a) Areas in PAG with increased responses in The Ice Man during cooling

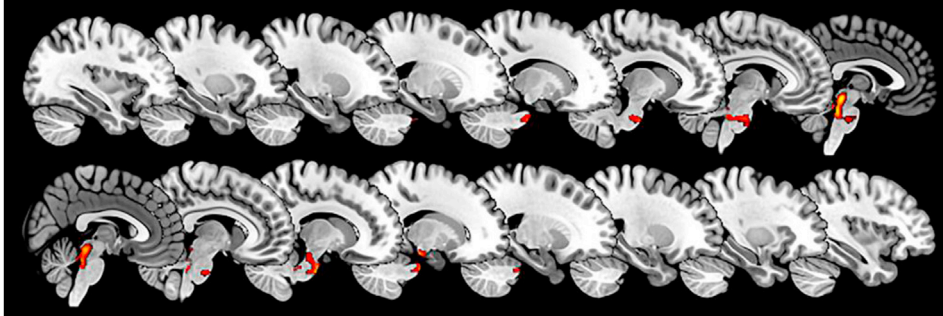

The mosaic of images above shows areas (warm colors) where The Iceman shows greater activity than normal controls during cooling. The graph at the right shows time series of activity from the cluster. The Iceman's data is shown under the red curve. Note the peaks in activation during periods of cooling (whereas the normal control line is flat). This suggests The Iceman's ability to regulate autonomous pain centers in periaqueductal gray matter.

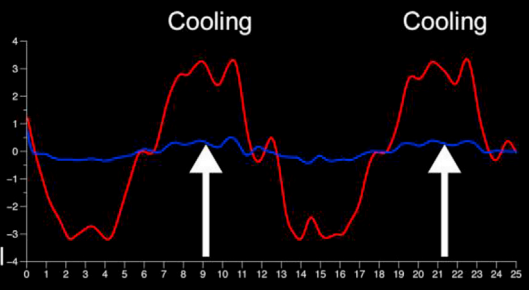

(b) Areas in the Insular Cortex with decreased responses in The Ice Man during cooling

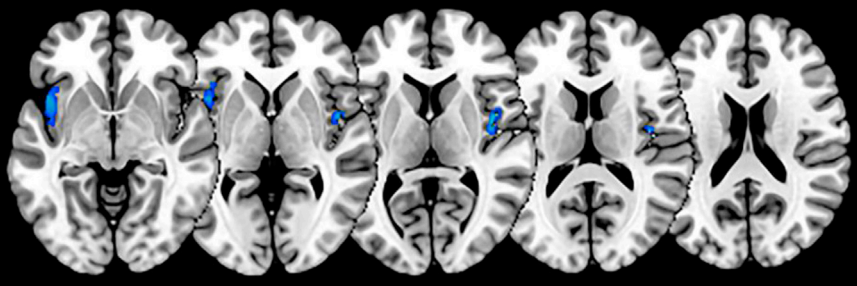

The mosaic of images above shows areas (cool colors) where The Iceman shows lower activity than normal controls during cooling. The graph at the right shows time series of activity drawn from the cluster. The Iceman's data is shown under the red curve. Note the troughs in activation during periods of cooling which are deeper than the normal controls. Note that The Iceman's activity in the insula (right) is in the opposite phase to his activity in periaqueductal gray matter (above, right).

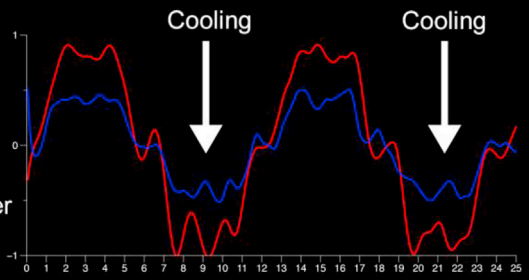

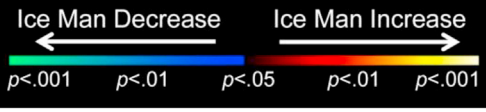

continued on next page

Fig. 3. fMRI results depicting brain activation and time series'. Following WHM, the Iceman showed greater range of fMRI responses in the periaqueductal gray matter during cooling periods (relative to rewarming), but less range of fMRI responses during cooling at the location of the insula. (a) Image mosaic displays areas (warm colors) where the Iceman showed greater activity than normal controls during cooling (arrow). The graph at the right shows the eigenvariate derived from the activation cluster. The Iceman's data is shown as the red curve (see text for LOESS smoothing details). Note the peaks in activation during periods of cooling (whereas the normal control line is flat). This suggests the Iceman's ability to regulate autonomous pain centers in periaqueductal gray matter using WHM. (b) Image mosaic shows areas (cool colors) where the Iceman showed lower activity than normal controls during cooling. The graph at the right shows the eigenvariate derived from the activation cluster. The Iceman's data is shown as the red curve. Note the troughs in activation during periods of cooling which are deeper than the normal controls. Moreover, the Iceman's activity in the insula is in opposite phase to his activity in periaqueductal gray matter.

Table 2
Brain areas showing significant differences in BOLD response between periods of cooling and warming observed in the "Iceman" as compared to the control group (N = 20).

Anatomical ROI	Critical Cluster Extent	Individual Cluster Extent	uncorrected *p*-value (T-value)	voxel peak (Tal)
Iceman WHM > Controls rest (Cooling > Warming) (Fig. 3)				
PAG	182	1022	<0.001 (4.86)	(-2, −31, −12)
Pons	182	367	<0.001 (4.76)	(14, −16, −32)
Iceman WHM > Controls rest (Warming > Cooling) (Fig. 4)				
mid Insula R	145	220	<0.001 (4.30)	(42, −3, 9)
ant Insula L	145	311	0.001 (3.70)	(-42,13, 2)

PAG: periaqueductal gray; ant: anterior; R: right; L: left, WHM: Wim Hof Method.

Table 3
Metabolic and thermoregulatory parameters during the mild-cold exposure PET study.

Parameter	Iceman	Controls	Assessment
BAT mass (g)	25	0–[26: **70**:95] - 182	low trend
BAT SUVmean	2.6	2.5–[4.0: **4.9**:5.9]–10.2	low trend
DEE rest (kcal/d)	1680	926–[1221: **1372**:1661] - 2395	high trend
DEE cold (kcal/d)	2080	1026–[1293: **1738**:2024]–2573	high trend
Δ DEE (%)	19	−38–[4: **7**:25]–42	comparable

Min – [quartile 1: median: quartile3] - max.

(26–95 g) of the control group (Table 3) and indicates an unremarkable activation of BAT for the Iceman. In contrast, both the resting DEE as well as cold exposure DEE were found to be above the interquartile range for the control group, although the % increase in DEE between rest and cold condition was comparable to that observed in the control group. These results indicate that resting DEE is increased in the Iceman, but is subject to a normal physiological response to cold exposure. Overall, the observed low BAT mass suggest that cold-activated BAT is not likely the source of increased DEE observed in the Iceman. As shown in Fig. 4B, the Iceman's SUVs in superficial (deltoid) and deep (psoas) muscles were both within the interquartile range of the control group. In contrast, SUVs for the superior and inferior intercostal muscles were found to be significantly increased in the Iceman, even though he was instructed not to apply WHM during the entire PET procedure. Finally, the Iceman's SUV in WAT showed a high trend (0.45, interquartile range 0.32–0.43), possibly due to increased perfusion of WAT during cold exposure.

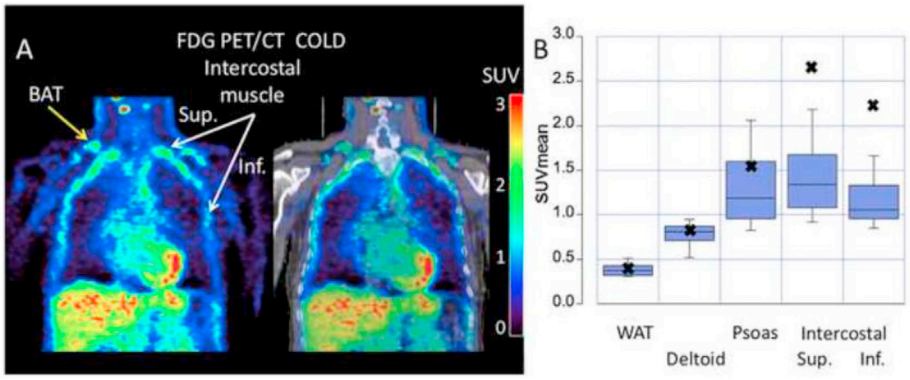

Fig. 4. (A) Representative coronal images showing FDG SUVs obtained for the Iceman (left) and the corresponding overlay with CT images (right). The images demonstrate limited FDG tracer uptake at the location of supraclavicular BAT (yellow arrow), however unusually high tracer uptake in both the superior and inferior intercostal muscle tissue (white arrow). (B) Boxplots showing the mean, interquartile range and extremes for SUVs derived from the control group in comparison to SUVs determined for the Iceman ("x") in various tissues. The plots demonstrate significantly higher SUVs in intercostal muscle as compared to the control group.

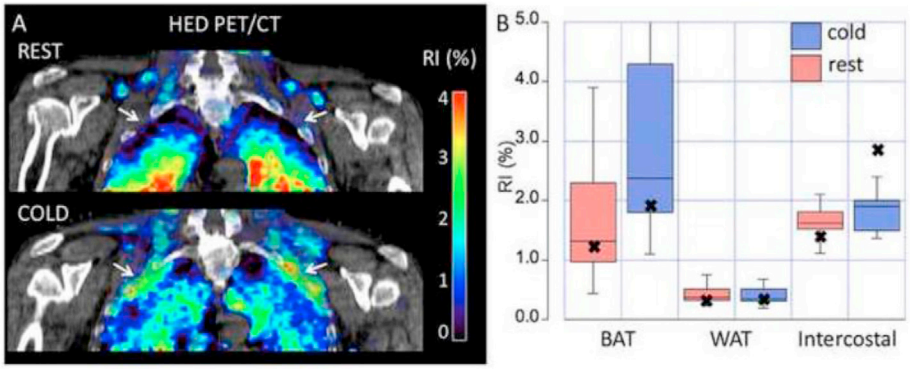

Fig. 5. (A) A significantly higher HED RI for the Iceman is depicted at the location of the superior intercostal muscle during the cold condition (but not during the resting condition). The HED RI for the Iceman during cold exposure was determined as 2.93%, which lies well outside the normative extremes (1.49–2.41%, median 1.90%). Based on our previously established relationship between HED RI and blood flow, these values for the superior intercostal muscle correspond to a resting perfusion of ~4 ml/100 g/min, which more than doubles during cold exposure (~10 ml/100 g/min) and corresponds to the low end of blood flow values observed in cold-activated BAT. (B) HED RI at the location of the Iceman's BAT and WAT ("x") were found to be within the corresponding normative interquartile ranges during both resting and cold conditions as were the HED RI values for superficial and deep muscle tissue.

Peripheral sympathetic innervation

Assessment of sympathetic innervation in peripheral tissues exhibited similar features to those observed for glucose metabolism. We determined a significantly higher HED RI for the Iceman at the location of the superior intercostal muscle during the cold condition, but not during thermoneutral condition (Fig. 5A). Compared to the control group, the Iceman's HED RI during cold exposure was determined as 2.93%, which lies well outside the normative extremes (1.49–2.41%, median 1.90%). Interestingly, during thermoneutral condition HED RI showed a low trend (1.29%) when compared to the normative extremes (1.11–2.05%, median 1.62%, Fig. 5B). Based on our previously established relationship between HED RI and blood flow (Muzik et al., 2017), HED RI values for the superior intercostal muscle correspond to a perfusion of ~4 ml/100 g/min, which more than doubles during cold exposure (~10 ml/100 g/min) and corresponds to the low end of blood flow values observed in cold-activated BAT. Finally, HED RI at the location of the Iceman's BAT and WAT were found to be within the corresponding normative interquartile ranges during both thermoneutral and cold conditions (Fig. 5B), as were the HED RI values for superficial and deep muscle tissue.

Discussion

Here we highlight what we believe are four important findings of our study pertinent to the physiological mechanism underlying the activity of the WHM: 1) Firstly, forceful respiration (deep inhalations and exhalations) followed by cold exposure and focused attention to one owns bodily state appears to activate primary control centers for descending pain/cold stimuli modulation in the PAG (Fig. 3a). This effect may possibly reflect a stress-induced analgesic response in the Iceman. 2) Secondly, the method also engages higher-order cortical areas (left anterior and right middle insula) that are associated with self-reflection and which facilitate internal focus as well as sustained attention in the presence of averse (e.g. cold) external stimuli (Fig. 3b). 3) Thirdly, forceful respiration results in increased sympathetic innervation and glucose consumption in intercostal muscle, generating heat that dissipates to lung tissue and warms circulating blood in the pulmonary capillaries (Figs. 4 and 5). This may counteract a decrease in core body temperature that otherwise would have occurred from cold exposure. 4) Finally, activation of supraclavicular BAT from increased sympathetic tone appears to have a negligible contribution to thermoregulation in the context of the WHM.

From our results we attempt to reconstruct a possible sequence of physiological events that might represent underlying mechanisms behind the capabilities of the WHM. We emphasize that our attempt to place our results within a physiological context constitutes a working hypothesis that still needs to be proven by future studies. However, we believe that providing this context is important to stimulate further discussion about the WHM. First, it appears that hyperventilation-induced activation of the sympathetic stress response primes the autonomic system through the release of stress hormones, with subsequent initiation of stress-induced analgesia mechanisms through a cold external stimulus. This mechanism might mediate the release of endogenous opioids/cannabinoids in both the periphery (via the descending pain/cold suppression pathway) and the CNS (via connections to the medial PFC, anterior cingulate and posterior insular cortex) leading to a feeling of euphoria, anxiolysis and a sense of well-being, which further promotes an attentionally focused (mindful) state that augments the analgesic effect of endocannabinoids. Though speculative, in the remainder of the Discussion, we provide ancillary evidence that supports these interpretations of our data.

Modulation of the cold response by respiration

When exposed to cold temperature, cold-sensitive transient receptor potential (TRP) neuronal cells in the periphery project to lamina I of the spinal cord where they synapse onto neurons that decussate and then ascend via the anterolateral fiber tract. This tract consists of three separate bundles: the spino-thalamic bundle (which terminates in the primary sensory cortex/insula and causes the "feeling" of cold), the spino-reticular bundle (which terminates in the reticular formation and initiates respiratory and cardiovascular changes) and the spino-mesencephalic bundle (which terminates in the PAG and modulates the perception of aversive stimuli) (Martin et al., 1999). Cold exposure activates sympathetic medullary nuclei such as the nucleus of the solitary tract (NST) and the parabrachial nucleus (PBN) that initiate adaptive changes in perfusion (vasoconstriction), and in respiratory pattern (increased pulmonary vascular resistance) via the release of stress hormones (cortisol and norepinephrine (NE)) that trigger system-wide changes in heart rate, blood pressure, metabolism and immune response.

The activity of the WHM method reverses the normal sequence of events: the unnatural respiratory pattern (hyperventilation with subsequent breath retention) causes hypocapnia and respiratory alkalosis, and is likely to initiate activation of the sympathetic stress response via chemoreceptors in the hypothalamus. Specifically, hyperventilation causes hypocapnia which in turn produces respiratory alkalosis, giving rise to the frequently reported lightheadiness, tingling in the arms and dizziness. Subsequent breath retention normalizes the relationship between blood O2 and CO2 levels through a severe decrease in oxygen saturation (<80%). This state mimics asphyxia and most likely initiates a sympathetic response in autonomic centers of the brainstem, most prominently the NST and PBN. The activity of these nuclei subsequently trigger systemic release of NE and cortisol via the HPA-axis, thus "priming" the system. Once primed, further stress escalation (cold exposure) is likely to initiate stress-induced analgesia by activating neurons in the PAG, triggering the release of endogenous opioids and cannabinoids that act both peripherally and centrally (Behbehani, 1995). Endogenous opioids activate the dorsolateral funiculus pathway that stimulates interneurons in lamina I of the spinal cord and prompting the release of enkephalins. Release of enkephalins in turn hyperpolarizes neurons that carry the initial stress (cold) signal from the periphery, thus decreasing the transmission of the external stimulus signal. As a result, perception of noxious external stimulus is decreased.

The patterns in our results generally fit these speculations. We demonstrate strong activation of the PAG during cold exposure when WHM is practiced, consistent with the release of endogenous opioids and endocannabinoids from this structure. Our results agree with earlier studies showing that aversive stimuli to the skin (thermal, mechanical or chemical) are particularly potent in activating endocannabinoid antinociception in higher cognitive areas (Calignano et al., 2000; Richardson et al., 1998). In contrast to opioids that cannot penetrate the blood-brain-barrier, endocannabinoids are lipids that readily cross the blood-brain-barrier and act centrally on cannabinoid type 1 (CB1) receptors that are densely expressed in brain regions implicated in the control of emotions and cognition (Glass et al., 1997). As such, binding to CB1 receptors might be the basis for the pleasurable feeling following various forms of stress-inducing activities (e.g. "runner's high") (Fuss et al., 2015) or the absence of pain during high-stress situations. Peripherally, endocannabinoids have been shown to act both as bronchodilators (Calignano et al., 2000) as well as vasodilators (Hillard, 2000; Wagner et al., 2001), thus promoting increased lung tissue perfusion as well as facilitating blood flow in the periphery. Together with our observation of increased intercostal muscle activity associated with greater heat production, the WHM may lead to improved heat exchange between lung tissue and blood, promoting increased perfusion of extremities during cold, thus ameliorating the dangers of tissue damage (such as frostbite) at the expense of irradiating a higher percentage of body heat. Additional and compelling evidence for such a mechanism is our observation of higher and unchanging skin temperature during the fMRI study when the Iceman practiced WHM (see Fig. 2), and the somewhat higher DEE observed during the thermoneutral condition.

Moreover, endocannabinoids inhibit oedema and inflammation (Richardson et al., 1998), which agrees well with previous reports that describe a decreased immune response associated with WHM practice (Kox et al., 2014). Along the same lines, endocannabinoids produce neither the respiratory depression nor the strong inhibition of GI motility that is associated with opioids. More importantly, it has been shown that endogenous cannabinoids produce analgesia after being released from activated neurons in the PAG (Walker et al., 1999). Electrical stimulation of the dorsal and lateral PAG produced CB1 cannabinoid receptor-mediated analgesia accompanied by a marked increase in the release of anandamide in the PAG, mediating behavioral analgesia (post-exercise calm, anxiolysis and a sense of well-being).

In addition to activations in the PAG, we also observed activation in the pons, proximate to the location of the pontine respiratory group (PRG). This area represents the body's pneumotaxic center, which is a network of neurons in the rostral dorsal lateral pons that regulates the depth and rate of respiration, and includes most prominently the suprabrachial and medial parabrachial nuclei. In the context of WHM, activation foci in the general vicinity of the PRG are not surprising, as a modified and highly controlled respiratory pattern is an essential component of this method. Furthermore, nuclei of the PRG receive input from chemoreceptors found in the carotid and aortic bodies, which detect changes in blood pH and subsequently regulate the activity of respiratory muscles, such as the diaphragm, the intercostal muscles as well as additional auxiliary muscles of the neck (the sternocleidomastoid and the scalene muscles). Our observation of increased sympathetic innervation of intercostal muscle complements the PRG activations and further highlights the central role of respiration within the WHM.

Our findings also demonstrate activations at the location of the left anterior and right middle insula. The bilateral insular cortex constitutes the main interoceptive brain region providing a sense of the physiological condition of the body (Craig, 2002, 2003). A posterior-to-anterior gradient in the insular cortex has been proposed, in which physical features of interoception are processed in the posterior insula and subsequently integrated with somatosensory, cognitive and motivational information in the middle and anterior portions of the insula (Craig, 2009, 2010). Thus, the insular cortex is crucial for the integration of bottom-up signals with top-down predictions from higher-level cortical areas, relaying internal needs to subjective awareness of feelings (Craig, 2002; Harrison et al., 2010; Gu et al., 2013). Notably, significant neural activation in the left anterior insula was reported as being uniquely associated with self-reflection (Modinos et al., 2009) and activation of the right middle insula has been observed in studies that investigated both body ownership and attribution of actions to oneself (Farrer and Frith, 2002). Given the importance of focused attention during the practice of WHM, the observed activations in self-referential brain areas are unsurprising and point towards the involvement of the salience brain network. By shifting attentional focus away from the activity of the default mode network (which might propagate the feeling of anxiety about future events and rumination about the past) and towards attention to the bodily sensation of focused respiration, this might produce a relaxation response that further enhances positive affective stimuli associated with cannabinoid release from the PAG. Interestingly, activations observed in the insular cortices were in opposite phase to those in the PAG, displaying a significantly lower BOLD signal that was contemporaneous with skin cooling for the Iceman as compared to the control group (Fig. 3B). This conforms well to previous reports (Muzik and Diwadkar, 2016; Craig, 2002; Calignano et al., 2000) suggesting that the insula contains a sensory representation of small-diameter afferent activity that relates to the physiological condition of the entire body, making discriminative thermal sensation possible. Therefore, the observed decreases in fMRI responses in the insular cortex may reflect a “turning down” of metabolic load as skin temperature decreases signal the onset of mild hypothermia.

Further considerations and limitations

In the absence of direct measurements of temperature from within the body itself, we are careful to note that our CNS effects must be narrowly related to the skin temperature changes that we directly measured, although the behavioral relevance of skin temperature changes is profound. Skin temperature represents an important auxiliary feedback signal to the main thermoregulatory system, reducing the system's response time and making core body temperature more stable (Romanovsky, 2007, 2014). Although skin temperature was monitored throughout the study and the observed skin temperature oscillations were found to be comparable during the thermoneutral condition among the control group and the Iceman, there might potentially exist differences in both temperature perception as well as in physiological responses to the periodic cooling and warming paradigm. This is substantiated by the fact that both the sympathetic innervation as well as glucose consumption were increased in the Iceman during prolonged exposure to mild cold (applied during the PET study), even though he was instructed not to engage in WHM and no observational indications of forced breathing were noted throughout the study. Thus, we can only speculate that long-term practice of the WHM predisposed the Iceman to a subconscious sympathetic reaction to a (relatively mild) cold exposure that resulted in a subclinical increase of intercostal muscle energy consumption. Moreover, it is likely that energy metabolism as well as heat production in intercostal muscle was further increased when the Iceman engaged the WHM. Another potential limitation of our study is the fact that the initial phase of the WHM includes the induction of hypocapnia in blood, in order to elicit activation of the sympathetic NS. The effects of pCO2 changes in blood on neuronal activity, oxidative metabolism and fMRI BOLD signal have been the subject of intensive discussion in the field (Zappe et al., 2008; Sicard and Duong, 2005). CO2 is a potent vasodilator and hypocapnia is known to cause a number of vascular changes in the brain (Kastrup et al., 1999; Rostrup et al., 2000). It is generally accepted that decreased CO2 levels in blood cause the brain to increase metabolism and spontaneous neural activity, and enter a higher arousal state (Xu et al., 2011). Although changes in CO2 during the fMRI scan cannot be completely excluded, it appears that CO2 and O2 values are likely to have normalized by the time the Iceman underwent the fMRI scan. This assumption is supported by the fact that no global differences were observed between the Iceman and the control group and by the observation of both positive (in PAG) as well as negative (in insula) changes in BOLD signal in our study. There is no clear explanation for why CO2 and O2 effects would selectively act on brain regions. Nevertheless, this should be acknowledged as an uncharacterized effect in our work.

Finally, our study's generalizability is also restricted by some temporal and spatial limitations inherent to fMRI (though these limitations are common to nearly all fMRI studies). Our spatial resolution was high relative to many studies (2×2 mm in-plane), yet precise anatomical location remains challenging because of variations in the intrinsic spatial resolution of brainstem nuclei. In particular, cellular differences in the brain stem are not easily distinguishable using conventional imaging methods (explaining the absence of well resolved anatomical masks). Thus, the designation of the exact anatomical location with respect to the observed significant activations in the pons region is challenging and one can only speculate with respect to the exact underlying mechanisms.

Conclusions

Our study provides an initial description of CNS processing during the practice of a technique that uses a combination of forced breathing and interoceptive focus that appears to allow a seasoned practitioner to withstand episodes of severe cold exposure. Our findings unequivocally demonstrate the activation of autonomic brain areas that are implicated in stress-induced analgesia as well as cognitive cortical areas that are associated with self-reflection. The observed strong activation of the PAG

might suggest the release of endogenous opiates/cannabinoids that mediate decreased sensitivity to cold exposure and promote a feeling of euphoria and well-being. Consequently, this technique might allow the practitioner to assert a higher level of control over key components of the brain's autonomous system.

Acknowledgements

This work was supported by the National Institute of Diabetes and Digestive and Kidney Diseases [grant number R01DK102455- 01]. We thank Dalal Khatib for help in data collection and Professor Richard Henson for valuable comments.

Appendix A. Supplementary data

Supplementary data related to this article can be found at https://doi.org/10.1016/j.neuroimage.2018.01.067.

Author contribution statement

OM and VD jointly designed, performed, analyzed and interpreted the research data.

Disclosure/conflict of interest statement

The authors declare no conflict of interest and nothing to disclose.

References

Allman, K.C., Wieland, D.M., Muzik, O., Degrado, T.R., Wolfe Jr., E.R., Schwaiger, M., 1993. Carbon-11 hydroxyephedrine with positron emission tomography for serial assessment of cardiac adrenergic neuronal function after acute myocardial infarction in humans. J. Am. Coll. Cardiol. 22, 368–375.

Behbehani, M.M., 1995 Aug. Functional characteristics of the midbrain periaqueductal gray. Prog. Neurobiol. 46 (6), 575–605. Review.

Calignano, A., La Rana, G., Loubet-Lescoulié, P., Piomelli, D., 2000. A role for the endogenous cannabinoid system in the peripheral control of pain initiation. Prog. Brain Res. 129, 471–482.

Cleveland, W.S., Devlin, S.J., 1988. Locally weighted regression: an approach to regression analysis by local fitting. J. Am. Stat. Assoc. 83, 596–610.

Craig, A.D., 2002. How do you feel? Interoception: the sense of the physiological condition of the body. Nat. Rev. Neurosci. 3, 655–666.

Craig, A.D., 2003. Interoception: the sense of the physiological condition of the body. Curr. Opin. Neurobiol. 13 (4), 500–505.

Craig, A.D., 2009 Jan. How do you feel–now? The anterior insula and human awareness. Nat. Rev. Neurosci. 10 (1), 59–70.

Craig, A.D., 2010. The sentient self. Brain Struct. Funct. 214 (5–6), 563–577.

Daanen, H.A., Van Marken Lichtenbelt, W.D., 2016. Human whole body cold adaptation. Temperature (Austin) 3 (1), 104–118.

Diwadkar, V.A., Murphy, E.R., Freedman, R.R., 2014. Temporal sequencing of brain activations during naturally occurring thermoregulatory events. Cerebr. Cortex 24, 3006–3013.

Eklund, A., Nichols, T.E., Knutsson, H., 2016. Cluster failure: why fMRI inferences for spatial extent have inflated false-positive rates. Proc. Natl. Acad. Sci. U.S.A. 113, 7900–7905.

Farrer, C., Frith, C.D., 2002. Experiencing oneself vs another person as being the cause of an action: the neural correlates of the experience of agency. Neuroimage 15 (3), 596–603.

Fuss, J., Steinle, J., Bindila, L., Auer, M.K., Kirchherr, H., Lutz, B., Gass, P., 2015. A runner's high depends on cannabinoid receptors in mice. Proc. Natl. Acad. Sci. Unit. States Am. 112 (42), 13105–13108.

Germano, G., Chen, B.C., Huang, S.C., Gambhir, S.S., Hoffman, E.J., Phelps, M.E., 1992. Use of the abdominal aorta for arterial input function determination in hepatic and renal PET studies. J NucI Med 33, 613–620.

Glass, M., Dragunow, M., Faull, R.L., 1997. Cannabinoid receptors in the human brain: a detailed anatomical and quantitative autoradiographic study in the fetal, neonatal and adult human brain. Neuroscience 77 (2), 299–318.

Gu, X., Hof, P.R., Friston, K.J., Fan, J., 2013. Anterior insular cortex and emotional awareness. J. Comp. Neurol. 521 (15), 3371–3388.

Hancock, A.M., Witonsky, D.B., Gordon, A.S., Eshel, G., Pritchard, J.K., Coop, G., Di Rienzo, A., 2008. Adaptations to climate in candidate genes for common metabolic disorders. PLoS Genet. 4, e32.

Harrison, A., Jolicoeur, P., Marois, R., 2010. "What" and "where" in the intraparietal sulcus: an FMRI study of object identity and location in visual short-term memory. Cerebr. Cortex 20 (10), 2478–2485.

Hillard, C.J., 2000. Endocannabinoids and vascular function. J. Pharmacol. Exp. Therapeut. 294 (1), 27–32.

Kastrup, A., Krüger, G., Glover, G.H., Neumann-Haefelin, T., Moseley, M.E., 1999. Regional variability of cerebral blood oxygenation response to hypercapnia. Neuroimage 10 (6), 675–681.

Kox, M., Stoffels, M., Smeekens, S.P., van Alfen, N., Gomes, M., Eijsvogels, T.M., Hopman, M.T., van der Hoeven, J.G., Netea, M.G., Pickkers, P., 2012. The influence of concentration/meditation on autonomic nervous system activity and the innate immune response: a case study. Psychosom. Med. 74 (5), 489–494.

Kox, M., van Eijk, L.T., Zwaag, J., van den Wildenberg, J., Sweep, F.C., van der Hoeven, J.G., Pickkers, P., 2014. Voluntary activation of the sympathetic nervous system and attenuation of the innate immune response in humans. Proc. Natl. Acad. Sci. U. S. A. 111, 7379–7384.

Lasker, G.W., 1969. Human biological adaptability. The ecological approach in physical anthropology. Science 166, 1480–1486. NY.

Lancaster, J.L., Tordesillas-Gutiérrez, D., Martinez, M., et al., 2007. Bias between MNI and Talairach coordinates analyzed using the ICBM-152 brain template. Hum. Brain Mapp. 28, 1194–1205.

Lubberink, M., Harms, H.J., Halbmeijer, R., de Haan, S., Knaapen, P., Lammertsma, A.A., 2010. Low- dose quantitative myocardial blood flow imaging using 15O-water and PET without attenuation correction. J. Nucl. Med. 51 (4), 575–580.

Martin, W.J., Coffin, P.O., Attias, E., Balinsky, M., Tsou, K., Walker, J.M., 1999. Anatomical basis for cannabinoid-induced antinociception as revealed by intracerebral microinjections. Brain Res. 822 (1–2), 237–242.

Modinos, G., Ormel, J., Aleman, A., 2009. Activation of anterior insula during self-reflection. PLoS One 4 (2), 1–8.

Muzik, O., Mangner, T.J., Granneman, J.G., 2012. Assessment of oxidative metabolism in brown fat using PET imaging. Front. Endocrinol. 3, 15–20.

Muzik, O., Mangner, T.J., Leonard, W.R., Kumar, A., Janisse, J., Granneman, J.G., 2013. 15O PET measurement of blood flow and oxygen consumption in cold-activated human brown fat. J. Nucl. Med. 54 (4), 523–531.

Muzik, O., Mangner, T.J., Leonard, W.R., Kumar, A., Granneman, J.G., 2017. Sympathetic innervation of cold-activated Brown and white fat in lean Young adults. J. Nucl. Med. 58 (5), 799–806.

Muzik, O., Diwadkar, V.A., 2016. In vivo correlates of thermoregulatory defense in humans: temporal course of sub-cortical and cortical responses assessed with fMRI. Hum. Brain Mapp. 37 (9), 3188–3202.

Ohtake, T., Kosaka, N., Watanabe, T., et al., 1991. Noninvasive method to obtain input function for measuring tissue glucose utilization of thoracic and abdominal organs. J. Nucl. Med. 32, 1432–1438.

Racimo, F., Gokhman, D., Fumagalli, M., Ko, A., Hansen, T., Moltke, I., Albrechtsen, A., Carmel, L., Huerta-Sanchez, E., Nielsen, R., 2017. Archaic adaptive introgression in TBX15/WARS2. Mol. Biol. Evol. 34 (3), 509–524.

Richardson, J.D., Kilo, S., Hargreaves, K.M., 1998. Cannabinoids reduce hyperalgesia and inflammation via interaction with peripheral CB1 receptors. Pain 75 (1), 111–119.

Romanovsky, A.A., 2007. Thermoregulation: some concepts have changed. Functional architecture of the thermoregulatory system. Am. J. Physiol. Regul. Integr. Comp. Physiol. 292, 37–46.

Romanovsky, A.A., 2014. Skin temperature: its role in thermoregulation. Acta Physiol. 210, 498–507.

Rosenspire, K.C., Haka, M.S., Van Dort, M.E., Jewett, D.M., Gildersleeve, D.L., Schwaiger, M., Wieland, D.M., 1990. Synthesis and preliminary evaluation of carbon-11-meta- hydroxyephedrine: a false transmitter agent for heart neuronal imaging. J. Nucl. Med. 31 (8), 1328–1334.

Rostrup, E., Law, I., Blinkenberg, M., Larsson, H.B., Born, A.P., Holm, S., Paulson, O.B., 2000. Regional differences in the CBF and BOLD responses to hypercapnia: a combined PET and fMRI study. Neuroimage 11 (2), 87–97.

Satinoff, E., 1978. Neural organization and evolution of thermal regulation in mammals. Science 201, 16–22. Review.

Sicard, K.M., Duong, T.Q., 2005. Effects of hypoxia, hyperoxia, and hypercapnia on baseline and stimulus-evoked BOLD, CBF, and CMRO2 in spontaneously breathing animals. Neuroimage 25 (3), 850–858.

Turner, R., Howseman, A., Rees, G.E., et al., 1998. Functional magnetic resonance imaging of the human brain: data acquisition and analysis. Exp. Brain Res. 123, 5–12.

van der Veldt, A.A., Hendrikse, N.H., Harms, H.J., Comans, E.F., Postmus, P.E., Smit, E.F., Lammertsma, A.A., Lubberink, M., 2010. Quantitative parametric perfusion images using 15O- labeled water and a clinical PET/CT scanner: test-retest variability in lung cancer. J. Nucl. Med. 51 (11), 1684–1690.

Vosselman, M.J., Vijgen, G.H., Kingma, B.R., Brans, B., van Marken Lichtenbelt, W.D., 2014. Frequent extreme cold exposure and brown fat and cold-induced thermogenesis: a study in a monozygotic twin. PLoS One 9 (7), e101653.

Wagner, J.A., Járai, Z., Bátkai, S., Kunos, G., 2001. Hemodynamic effects of cannabinoids: coronary and cerebral vasodilation mediated by cannabinoid CB(1) receptors. Eur. J. Pharmacol. 423 (2–3), 203–210.

Walker, J.M., Huang, S.M., Strangman, N.M., Tsou, K., Sañudo-Peña, M.C., 1999. Pain modulation by release of the endogenous cannabinoid anandamide. Proc. Natl. Acad. Sci. U. S. A. 96 (21), 12198–12203.

Ward, B.D., 2000. Simultaneous Inference for fMRI Data. Medical College of Wisconsin, Milwaukee, WI.

Xu, F., Uh, J., Brier, M.R., Hart Jr., J., Yezhuvath, U.S., Gu, H., Yang, Y., Lu, H., 2011. The influence of carbon dioxide on brain activity and metabolism in conscious humans. J. Cerebr. Blood Flow Metabol. 31 (1), 58–67.

Xu, X., Karis, A.J., Buller, M.J., Santee, W.R., 2013. Relationship between core temperature, skin temperature, and heat flux during exercise in heat. Eur. J. Appl. Physiol. 113 (9), 2381–2389.

Zappe, A.C., Uludağ, K., Oeltermann, A., Uğurbil, K., Logothetis, N.K., 2008. The influence of moderate hypercapnia on neural activity in the anesthetized nonhuman primate. Cerebr. Cortex 18 (11), 2666–2673.